Optical Engineering

OpticalEngineering.SPIEDigitalLibrary.org

High-speed focus servo control system using Nyquist aperture mounted on a triaxial actuator for holographic disc drive system

Yukinobu Tanaka
Tatsuro Ide
Jiro Hashizume

SPIE.

Yukinobu Tanaka, Tatsuro Ide, Jiro Hashizume, "High-speed focus servo control system using Nyquist aperture mounted on a triaxial actuator for holographic disc drive system," *Opt. Eng.* **59**(3), 035105 (2020), doi: 10.1117/1.OE.59.3.035105

High-speed focus servo control system using Nyquist aperture mounted on a triaxial actuator for holographic disc drive system

Yukinobu Tanaka,[a,*] Tatsuro Ide,[b] and Jiro Hashizume[c]
[a]Hitachi Ltd., Center for Exploratory Research, Saitama, Japan
[b]Hitachi Ltd., Center for Technology Innovation – Electronics, Tokyo, Japan
[c]Hitachi Ltd., Center for Technology Innovation – Mechanical Engineering, Ibaraki, Japan

Abstract. We have developed a holographic data storage system using angular-multiplexing recording that has a large capacity of 2 TB and a data transfer rate of 1 Gbit/s. To read a hologram recorded on a holographic disc at high speed, it is necessary to control the relative position shift between a hologram recorded on a disc and a readout optical system. However, in angular-multiplexing data storage systems, the optical system has no moving mechanism, unlike conventional optical discs such as Blu-ray Discs™. Therefore, it is difficult to control the disc position with high precision and to reduce the settling time of the positioning because the holographic disc has no physical structure for the position control mechanism to control the relative position shift. In the systems, a disc mounted on a disc stage is moved to a position where the signal-to-noise ratio of the reproduced hologram becomes the maximum value. Hence, we present a servo control system based on a shift of the Nyquist aperture using a real-time position error signal to control the disc position. In experiments, a positioning accuracy of ± 15 μm and a settling time of 8.5 ms for our angular-multiplexing data storage system using a nonlinear parabolic focus position error signal have been observed. [DOI: 10.1117/1.OE.59.3.035105]

Keywords: holographic; servo control; angular-multiplexing; focus; Nyquist aperture; storage system.

Paper 191491 received Oct. 29, 2019; accepted for publication Mar. 9, 2020; published online Mar. 27, 2020.

1 Introduction

The continuing exponential growth in the total amount of worldwide archival data is sometimes referred to as an information explosion. It is expected that the total data size in 2020 will be 44 ZB.[1] A promising approach to ecofriendly archival storage is the use of optical discs due to their large capacity, low running cost, and longevity. However, while their capacity can be readily expanded by increasing the number of recording layers,[2–4] the groove structure needed for tracking control increases the disc fabrication cost.[5] Thus, using a multilayer optical disc increases the cost. One solution to this problem is to use a separate guide layer with a groove structure and multiple recording layers without a groove structure.[6–8] This simple disc structure reduces the disc fabrication cost because the process of forming a groove structure on the recording layers is eliminated. However, the practical data transfer rate is thought to be around megabits per second[9] because recorded data are accessed sequentially (bit-by-bit).

Another solution is to use holographic memory, which has a fast transfer rate in the gigabit-per-second class and a large disc capacity in the terabyte class.[10–13] It is regarded as one of the most promising candidates for the next generation of optical discs. In the memory, a few megapixels of two-dimensional data, called a page, are recorded in one exposure. A page is recorded in an interference pattern between a signal beam and a reference beam as a hologram in photosensitive materials, and hundreds of pages can be multiplexed at a single location with angular-multiplexing[14–18] or shift-multiplexing (coaxial holography).[19–21] In holographic data storage

*Address all correspondence to Yukinobu Tanaka, E-mail: yukinobu.tanaka.kt@hitachi.com

systems (HDSS), we think that the use of angular multiplexing is more effective than shift multiplexing in terms of volume use efficiency because it enables effective utilization of a thick disc, thus achieving a higher recording density.[22–25]

We have been developing an angular multiplexing HDSS. Tables 1 and 2 list the system specifications required for a 2-TB disc capacity and a 1-Gbit/s data transfer rate based on the results of our research, simulated and experimental results, respectively.[26] In Table 2, the access times between pages and between books (clusters of hundreds of pages, in our case, one book consists of 440 pages) are determined by the mechanical moving time of a galvanometer and settling time of the stepwise movement of a spindle motor in stop-and-go sequences.

To realize an HDSS that satisfies these specifications, it was necessary to develop fast and precise positioning control mechanisms. For example, during the recording process, a book is recorded by angular multiplexing in a single volume. Each multiplexed data page can be reproduced by changing the incident angle of a reference beam by a galvanometer in order to maximize the signal-to-noise ratio (SNR) of a target hologram during the reproduction process, where SNR expresses the reproduction quality of a reproduced hologram (hereafter called a target hologram). Therefore, we developed a high-speed reference beam angle control mechanism in order to access a reproduced data page quickly and precisely.[27] As a result, we demonstrated multiple sequential moving control processes between each page within 300 μs/page with less than ± 3.0 m deg in an actual experimental system.

Table 1 System specifications for 2-TB disc capacity.

Disc capacity	TB	2
Disc recordable area	mm^2	11,464
Disc diameter	mm	135
Disc usage efficiency	%	0.88
Recording density	$Tbit/in.^2$	2.4
Page capacity	Mbit	2.7
Multiplexed page numbers	—	440
Book size	mm^2	0.32
Code rate	—	0.44

Table 2 System specifications for 1-Gbit/s transfer rate in reproduction.

Transfer rate in reproduction	Gbit/s	1
Disc capacity	TB	2
Total data reproduction time	min	186
Book number per disc	—	31,693
Access time between books	ms	22
Multiplexed page numbers	—	440
Exposure time	ms	0.3
Access time between pages	ms	0.3
Adjustment time	min	81

To realize fast access times between books, it is necessary to control the relative position shift between a target hologram and an optical system (hereafter called an optical unit) of the HDSS. A solution to control the relative position shift is to use a separate guide layer with a groove structure, which is necessary for the position control mechanism[9] that is independent of the recording layer without a groove structure.[28] However, a signal beam and a reference beam reflect diffusely with the groove structure, and the scattered beam becomes noise when a hologram is recorded. As a result, the SNR of the target hologram decreases. Hence, we have developed a new disc-positioning mechanism without having a special layer with the groove structure. This new disc positioning is performed by controlling the position of a Nyquist aperture (NyA) mounted on a triaxial actuator based on real-time triaxial position error signals (PESs). The PESs are direct signals obtained from a target hologram. The position shift of the NyA is controlled along the focal, tangential, and radial axes based on each PES using the triaxial actuator. The PESs express the triaxial residual error of the reference beam from the target hologram. One of the triaxial PESs, the PES of the focal axis, is a nonlinear parabolic function. In addition, in order to achieve a 1-Gbit/s data transfer rate, it was necessary to develop the fast focus servo control system, which is the slowest compared to the other axes. In the case of the nonlinear parabolic function, the direction to move the NyA cannot uniquely be determined from the intensity of the PES of the focal axis. This is because the PES gives the same value for two different NyA positions other than the origin. Therefore, to determine the moving direction of the NyA, an additional sensor is necessary or else it is necessary to perform complicated linearization processing. In this paper, we propose a new focus servo control system using the PES of the nonlinear parabolic function without adding a further sensor and performing complicated linearization processing.

In Sec. 2, our conventional disc-positioning mechanism and the features are described. In Sec. 3, problems of the conventional disc-positioning mechanism are clarified. In Sec. 4, we present a new servo control system based on a shift of the NyA using a real-time PES to control the disc position. In Sec. 5, results and discussion concerning positioning accuracy and settling time are described. Finally, Sec. 6 concludes with a brief review of our developed servo control system.

2 Disc-Positioning Mechanism

A schematic illustration of the disc-positioning mechanism using a disc stage is shown in Fig. 1. The focal (or z) axis is taken as the direction of disc thickness, the Bragg (or y, hereafter called "tangential") axis is taken as the direction in which the reference beam angle is changed for multiplexing, and the pitch (or x, hereafter called "radial") axis is taken as the direction perpendicular to both the focal and tangential axes.

In our developed HDSS, the optical unit has no moving mechanism, and a disc mounted on a disc stage moves to a position where the SNR of the target hologram becomes the maximum value. The disc stage consists of a sled stage, radial stage, spindle motor, focal stage, and tangential stage. Therefore, the disc stage has five movable axes, which are the sled, radial, rotation, focal, and tangential axes. The disc positioning is performed by moving the disc stage.

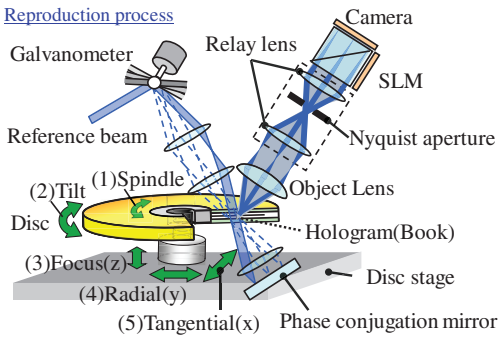

Fig. 1 Schematic illustration of the disc-positioning mechanism.

The sled stage is the mechanical stage for loading the disc into the HDSS. The radial stage moves a disc to the radial axis and changes radius r at the disc. To access a target book, the spindle motor rotates the disc and changes rotation angle θ at the disc. In the disc positioning, radius r and rotation angle θ determine the disc in-plane positioning. The focal stage moves the disc to the focal axis of the disc thickness. The tangential stage moves the disc to the tangential axis. The tangential and radial stages have two orthogonal axes and are controlled to compensate for the eccentricity of a disc. By appropriately controlling the tangential and radial stages, the effect of the eccentricity is cancelled, and a hologram is written or reproduced in the correct position. Furthermore, the disc-positioning mechanism is also equipped with two edge sensors for eccentricity compensation and a rotary encoder for controlling rotation angle θ of the spindle motor.

3 Problems with Conventional Disc-Positioning Mechanism

During the reproduction process, the reference beam is irradiated to the disc as its angle is changed by a galvanometer. The reference beam that penetrated the disc is reflected by the phase conjugation mirror and irradiated to the disc again. The readout beam diffracted from a target hologram by the reference beam is focused by a relay lens, and the beam passes the NyA. The NyA is placed in the Fourier plane of the relay lens. The readout beam from the target hologram reaches the camera and is consequently captured by the camera. The SNR of the target hologram is calculated from the captured camera image. The SNR defined in Eq. (1) was utilized as the evaluation index of the signal quality of the images:[29]

$$\mathrm{SNR} = 20\log_{10}\left(\frac{\mu_{\mathrm{on}} - \mu_{\mathrm{off}}}{\sigma_{\mathrm{on}} + \sigma_{\mathrm{off}}}\right)\ (\mathrm{dB}), \tag{1}$$

where μ_{on} and μ_{off} are the mean values and σ_{on} and σ_{off} are the variances of "on" and "off" pixels.

A serious problem with the conventional disc-positioning mechanism is shown in Fig. 2. The amount of each relative position shift Δ of the focal, tangential, and radial axes is represented as $\Delta_{\mathrm{defocus}}$, Δ_{tan}, and Δ_{rad}, respectively. The target hologram and the optical unit are aligned as shown in Fig. 2(a). The essential function of the NyA is to block off undesired readout beams from neighboring books during the reproduction process. However, when the hologram is off the expected position, part of the readout beam is interrupted by the NyA and does not reach

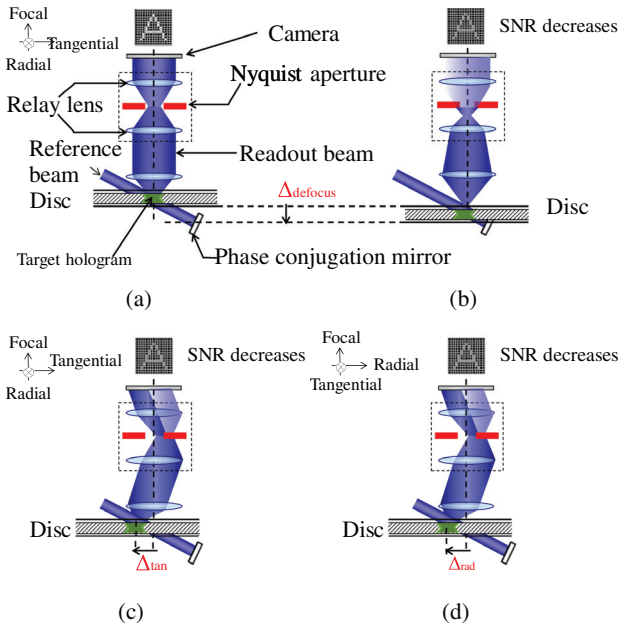

Fig. 2 Conventional disc stage control mechanism: (a) correctly aligned, (b) misaligned ($\Delta_{\mathrm{defocus}}$), (c) misaligned ($\Delta_{\mathrm{tan}}$), and (d) misaligned ($\Delta_{\mathrm{rad}}$).

the camera as shown in Figs. 2(b)–2(d). As a result, the SNR of the target hologram decreases. To compensate for the lower SNR caused by the NyA position, a disc mounted on a disc stage moves to a position where the SNR of the target hologram becomes the maximum value. The positioning accuracy of the disc can be less than several μm. However, the positioning of the disc stage is not performed by the readout beam, but by the encoder on the inner circumference of the disc. Even if the position of the disc can be controlled with high precision, a position shift with respect to the target hologram occurs. Therefore, since the positioning of the disc stage control is not performed based on the target hologram, a position shift of about 50 μm occurs at the maximum. This is because the physical structure that existed on conventional optical discs such as Blu-ray Discs™ is not formed on our holographic disc. This is because not only is scattering of light caused by forming a physical structure but also because constructing a physical structure on the disc reduces the capacity of the disc. Therefore, there was no way to know the displacement in real time. In other words, a serious problem is that high-speed and accurate positioning on a plain disc is required.

4 New Disc-Positioning Mechanism

We have devised a new disc-positioning mechanism to compensate for the relative position shift Δ by moving the position of the NyA that interrupts part of the readout beam. The method relaxes the severe positional tolerance of the holographic disc so that a coarse positioning control performed by spindle or sled motors conventionally can be sufficient for the positioning of the holographic disc. For example, when the relative position shift Δ_{defocus} is 0 μm in Fig. 3(a), the readout beam passes the NyA. In contrast, as shown in Fig. 3(b), if the relative position shifts $\Delta_{\text{defocus}} \neq 0$ μm, part of the readout beam is interrupted by the NyA and does not reach the camera and the SNR decreases. The width of the NyA was set to be 1.14 times larger than the Nyquist size D_{NyA}, which is defined as

$$D_{\text{NyA}} = \frac{\lambda f_r}{P_{\text{SLM}}}, \tag{2}$$

where P_{SLM} is the spatial light modulator (SLM) pixel pitch, λ is the wavelength, and f_r is the focal length of the relay lens.

As shown in Fig. 3(c), it can relax the severe tolerance of the positioning during readout if the relative position shift Δ_{defocus} from the expected position of the disc can be adjusted by moving the NyA position to target displacement $\Delta_{\text{defocus}'}$ to prevent the deterioration caused by the vignetting of the readout beam at the NyAeA with Δ_{defocus} and to allow the readout beam to pass through the NyA instead of carrying out precise positioning control of the disc. The relative position shift $\Delta_{\text{defocus}'}$ of the NyA is determined by the magnification calculated using the ratio of the focal length of the relay lens f_r to that of the objective lens f_0:

$$\Delta_{\text{defocus}'} = \left(\frac{f_r}{f_0}\right)^2 \times \Delta_{\text{defocus}}. \tag{3}$$

As shown in Figs. 3(d) and 3(f), $\Delta_{\text{rad}'}$ and $\Delta_{\text{tan}'}$ are similarly expressed as

$$\Delta_{\text{rad}'} = \frac{f_r}{f_0} \times \Delta_{\text{rad}}, \quad \Delta_{\text{tan}'} = \frac{f_r}{f_0} \times \Delta_{\text{tan}}, \tag{4}$$

where $\Delta_{\text{defocus}'}$ is a square because $\Delta_{\text{defocus}'}$ is a longitudinal magnification. The optical parameters used in this study (summarized in Table 3) were determined experimentally.[30,31] For example, when $f_r = 40$ mm, $f_0 = 12.4$ mm, and the relative position shift of the disc Δ_{defocus} remains at 50 μm, we should move the NyA $\Delta_{\text{defocus}'} = 520$ μm in the focal axis to ensure high readout quality.

The new mechanism can control the disc position quickly and precisely because the position of the NyA is controlled based on a real-time PES obtained from the target hologram. Moreover, the weight of the holographic disc is about 100 g and that of the NyA is <1 g (summarized in

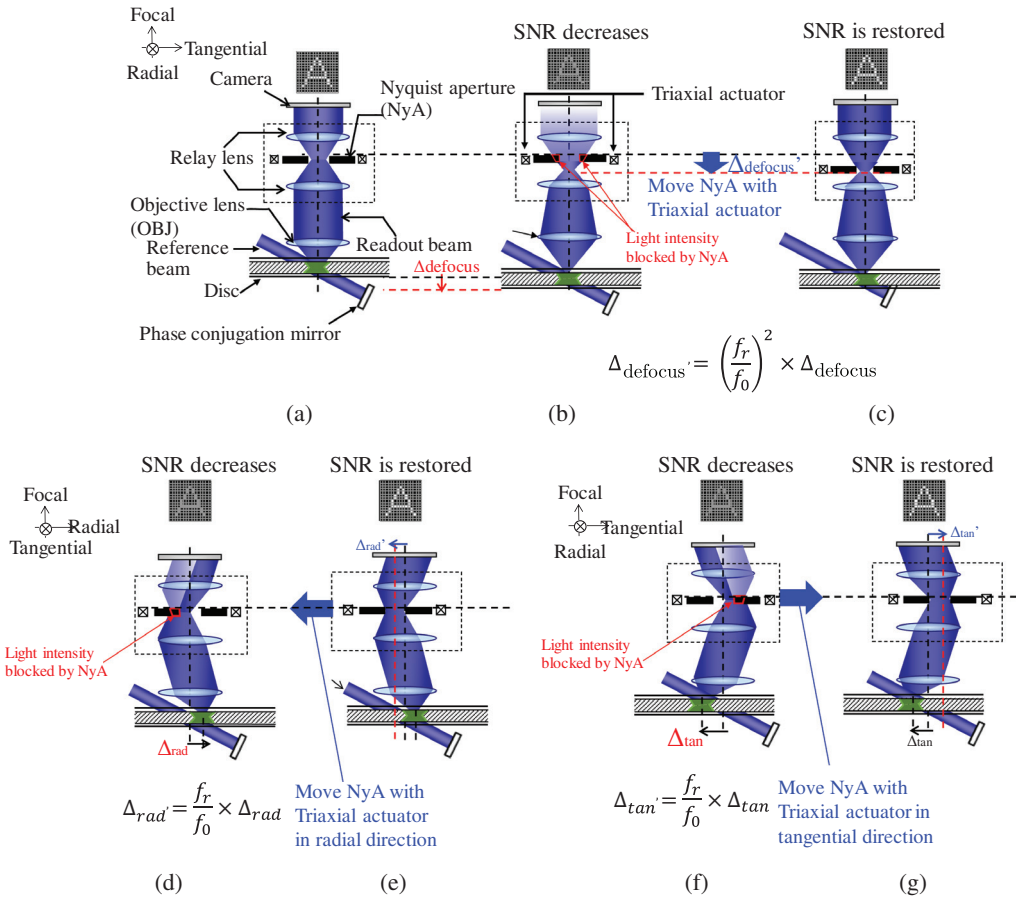

Fig. 3 Disc stage control mechanism: (a) correctly aligned position, (b) disc position was shifted by $\Delta_{defocus}$ from correctly aligned position, decreased SNR, (c) moving triaxial actuator in focal direction, depending on light intensity blocked by NyA, improves SNR, (d) disc position was shifted by Δ_{rad} from correctly aligned position, (e) moving triaxial actuator in radial direction, depending on light intensity blocked by NyA, improves SNR, (f) disc position was shifted by Δ_{tan} from correctly aligned position, and (e) moving triaxial actuator in tangential direction, depending on light intensity blocked by NyA, improves SNR.

Table 3 Optical parameters.

Item		Symbol	Value	Unit
Wavelength		λ	405	nm
Reference beam angle		θ	48	deg
Objective lens (OBJ)		Numerical aperture	0.6	—
Focal length of OBJ		f_0	12.4	mm
Focal length of RL		fr	40	mm
SLM	Pixel number	N_{SLM}	1944	pixel
	Pixel pitch	P_{SLM}	7.8	μm

Table 4). Compared with the size and weight of the holographic disc, those of the NyA can be markedly reduced, which is advantageous for realizing fast readout. Furthermore, there is another advantage in that the compensation method has high affinity with the objective lens actuator for conventional optical disc drive systems, such as DVDs and Blu-ray discs™.

Table 4 Experimental parameters.

Item		Value	Unit
Holographic disc		100	g
Recorded hologram	Width in radial h_r[a]	0.8	mm
	Width in radial h_t[a]	0.7	mm
Nyquist aperture	Width in radial w_{NyAr}	2.4	mm
	Width in tangential w_{NyAt}	1.2	mm
	Weight M_{NyA}[b]	<1	g

[a]Width in the middle of the depth of the holographic disc.
[b]Including NyA holder.

4.1 *Required Specification of the New Positioning Mechanism*

First, we allocated the margin or fixed tolerance by distributing the amount of allowable unique noise to each stress. In the margin allocation, the SNR was utilized as the evaluation index of the signal quality of a target hologram. From the simulation and experimental results, in this distribution of unique noise, the allowable total unique noise of the new disc-positioning mechanism was assigned to be 8.2%,[26] where the total unique noise is the square-root of the sum of the squares of each unique noise. The unique noise generated by the new positioning mechanism is related to the presence of a positioning error of each axis.

Next, specifications of a positioning accuracy required for the new mechanism are described. As mentioned in Sec. 1, we explain the specification of focal axis in particular in this paper. The relationship between relative position shift $\Delta_{defocus}$ and SNR is calculated using an optical simulator.[30] The optical parameters used in this study (summarized in Table 3) were determined experimentally. The results of optical simulation confirmed that the new disc-positioning mechanism is effective, as shown in Fig. 4. Figure 4 plots the relationship between the relative position shift $\Delta_{defocus}$ and the SNR, where the solid line indicates the SNR without the new disc-positioning mechanism and the dashed line indicates the SNR with the new mechanism. When the relative position shift $\Delta_{defocus} \leq 20$ μm, it is clear from the SNR indicated by the solid line that the SNR is less than about 0.1 dB. This SNR when the relative position shift $\Delta_{defocus} \leq 20$ μm can be compensated for by signal processing. However, when the relative position shift $\Delta_{defocus} > 20$ μm, the SNR was degraded by -5 dB when the $\Delta_{defocus}$ was 100 μm. Therefore, the new disc-positioning mechanism demands a positioning accuracy of 20 μm. On the other hand, we can see from the SNR indicated by the dotted line that if the relative position shift

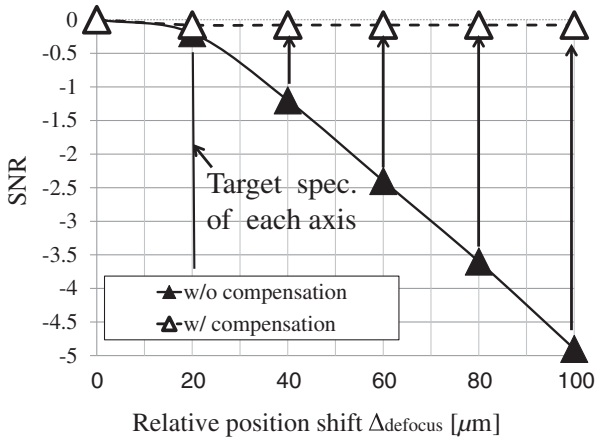

Fig. 4 Relationship between $\Delta_{defocus}$ and SNR: relationship between relative position shift $\Delta_{defocus}$ and SNR.

Δ_{defocus} from the expected position of the disc can be adjusted by moving the NyA position target displacement $\Delta_{\text{defocus}'}$, it is possible to improve the SNR at the position of the NyA even though the position of the disc does not shift to compensate for the relative position shift Δ_{defocus}. The reason for the decrease in SNR is that part of the readout beam from the target hologram is interrupted by the NyA. Hence, it was revealed that a similar compensation effect is provided by moving the position of the NyA.

As mentioned above, the new positioning mechanism needs to keep the unique noise below 8.2%. Figures 5(a) and 5(b) show the change in unique noise for the Δ_{defocus}, Δ_{tan}, and Δ_{rad}. If the focal axis is 20 μm, the unique noise will be 6% in Fig. 5(a). If the target relative position shit between the tangential axis and the radial axis is designed to be 5 μm, the unique noise is 2% and 5% in Fig. 5(b), respectively. For example, since the unique noise is independent noise, if the unique noise of each axis is 6% (Δ_{defocus}), 5% (Δ_{tan}), and 2% (Δ_{rad}), the total unique noise is about 8% $[= \sqrt{(6^2 + 5^2 + 2^2)}]$. As a result, the new positioning mechanism satisfies 8.2% of the specification value.

The data transfer rate in reproduction $\text{TR}_{\text{d\_repro}}$ is calculated as

$$\text{TR}_{\text{d\_repro}} = \frac{C_d}{T_{\text{d\_repro}} + T_A}, \tag{5}$$

where $T_{\text{d\_repro}}$ is the total data reproduction time and T_A is the time for adjustments performed to minimize disc displacement by controlling the position of the disc and to compensate for Bragg mismatch caused by the temperature change. The disc capacity of the HDSS, C_d, is given as

$$C_d = S_d \times R_d \times \text{dens} \times R_c, \tag{6}$$

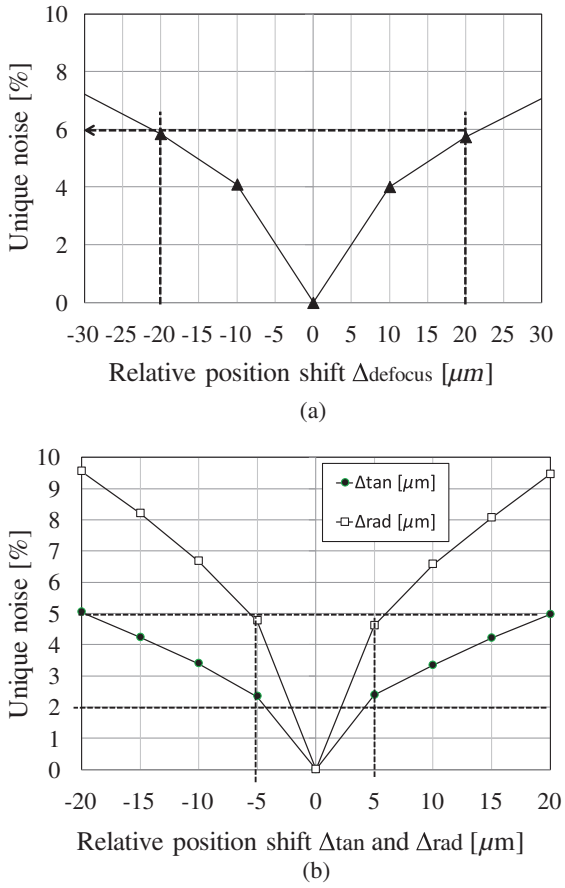

Fig. 5 Relationship between relative position shift Δ and unique noise: (a) relationship between Δ_{defocus} and unique noise and (b) relationship between Δ_{tan}, Δ_{rad}, and unique noise.

Table 5 Specifications of new disc-positioning mechanism required for 1-Gbit/s transfer rate in reproduction.

	Symbol	Unit	Conventional disc-positioning mechanism	New disc-positioning mechanism
Total adjustment time required for 1 Gbps	T_A	min	81	81
(1) Book number per disc	B_{repro}	—	31,693	31,693
(2) Focus servo	T_F	ms/book	300	10
	—	min	158 ($= B_{repro} T_F$)	5
(3) Tangential servo	T_T	ms/book	200	10
	—	min	106($= B_{repro} T_T$)	5
(4) Radial servo	T_R	ms/track	300	200
	—	min	0.2 ($= 47\, T_R$)	0.2
(5) Adjustment time		min	70	70

where S_d is the disc recordable area, R_d is the disc usage efficiency, and R_C is the code rate (summarized in Table 1). As indicated in Table 5, total adjustment time required for 1 Gbit/s is 81 min. However, as indicated in Table 5, the conventional disc-positioning mechanism requires 334 min $[= B_{repro}(T_F + T_T) + 47T_R + T_{adj}]$ for the T_A, where T_F, T_T, and T_R are the setting times of the focus, tangential, and radial servo control system, respectively. T_R is determined to be 47 times, which is the number of the radius movements. In this case, the data transfer rate of our HDSS is 0.5 Gbit/s. As shown in Fig. 6, the total setting time of the new disc-positioning mechanism needs to be 254 min shorter. To increase the transfer rate to 1 Gbit/s, we designated the specifications of the new disc-positioning mechanism in Table 6.

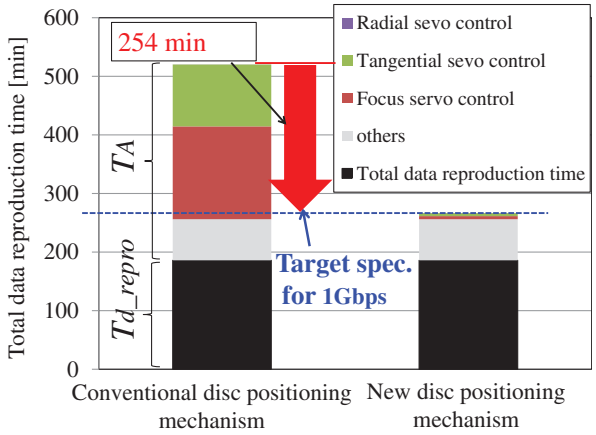

Fig. 6 Specifications of the disc-positioning mechanism required for 1-Gbit/s transfer rate in reproduction.

Table 6 Specification of positioning control system.

Control axis	Tolerance (μm)	Settling time (ms)
Defocus	±20	≦10
Tangential detrack	±5	≦10
Radial detrack	±5	≦200

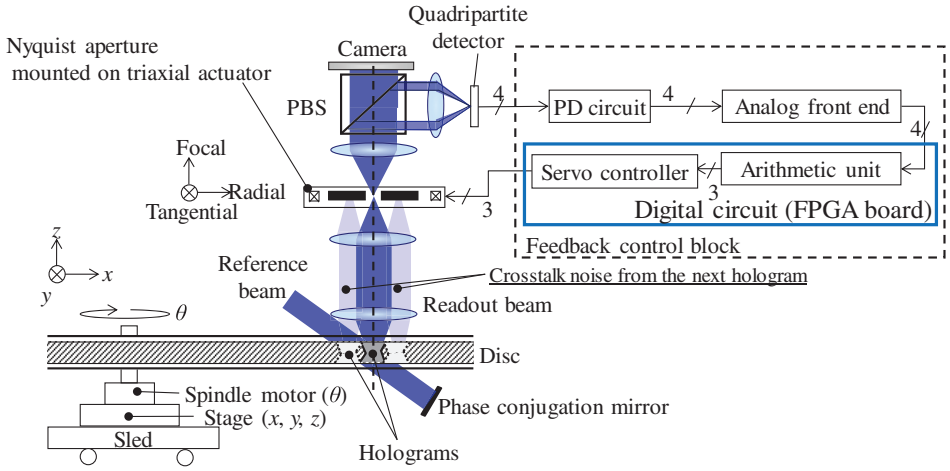

Fig. 7 Schematic illustration of developed servo control system.

4.2 *Developed Servo Control System*

A schematic illustration is shown in Fig. 7 of the high-precision and fast servo control system developed to compensate for the residual relative position shift Δ caused by the disc-positioning mechanism. The servo control system consists of two blocks. One is composed of the disc-positioning mechanism and the other is composed of a new NyA unit mounted on a triaxial actuator, an optical block for detecting real-time PESs, and a feedback control block based on their PESs. A PES expresses the position error of the reference beam from the target hologram. The feedback control block consists of an analog circuit block and a digital circuit block. The digital circuit was built with a field programmable gate array board [ACM-022 (CycloneIII), HuMANDATA Ltd.].

The intensity of PES to detect the PESs is shown in Fig. 8. The optical block consists of four half-wave plates (HWPs), a polarized beam splitter (PBS) prism, and a quadripartite photo detector (four-channel PD), where a tangential error signal (TES), focus error signal (FES), and radial error signal (RES) are the respective PESs of the tangential axis, focal axis, and radial axis. In order to move the NyA at high speed, the lightweight HWP is placed around the NyA instead of

Servo light	Readout beam incident on periphery of Nyquist aperture
Detection method	*X*/*Y* : Differential (Left/Right, Up/Down) *Z* : Total
Schematic optics (readout)	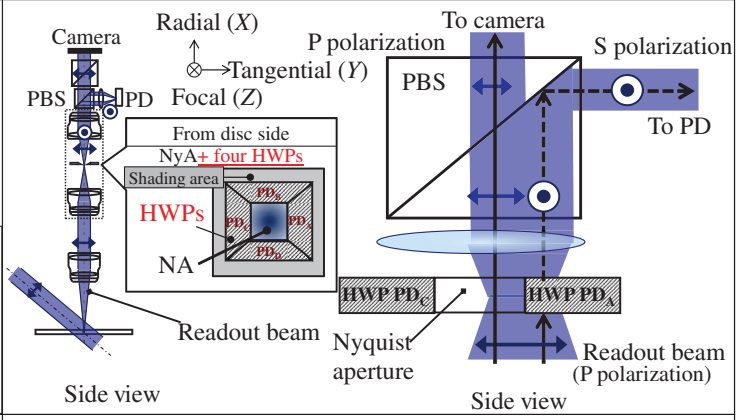
FES: Focus error Signal PES: Position error Signal HWP: Half-Wave Plate TES: Tangential error signal RES: Radial error signal	
Error signal	$TES = PD_A - PD_C$, $RES = PD_B - PD_D$, $FES = PD_A + PD_B + PD_C + PD_D$

Fig. 8 Optical block.

putting the PD onto the NyA. The intensity of PES is composed from those on the area of the HWP.

The new NyA fulfills both the function of extracting the intensity of the readout beam illuminating the outer area of the NyA area to generate the PESs and the original function of the NyA aperture explained in Sec. 3. The NyA is composed of two regions in Figs. 9(a) and 9(b). Figure 9(a) is a side view of the new NyA, Fig. 9(b) shows a top view as viewed from the disc side, and a four-channel PD converts light photons into the current detected by each channel and outputs four currents, which are called PD_A, PD_B, PD_C, and PD_D in Fig. 9(c). The first region is merely a transparent area that plays the original role of the NyA. The *P*-polarized readout beam passing through the first region is passed through a PBS prism and is then incident on the camera, as shown in Fig. 7. The second region surrounding the first region of the NyA consists of an HWP. The *P*-polarized readout beam passing through the second region is reflected by the PBS prism because the polarization direction is changed from *S* to *P* by the HWP and is then incident on the four-channel PD to generate the PESs. Figure 9(d) shows a diagram of the situation in which the *S*-polarized readout beam illuminates the four-channel PD when the relative position shift Δ_{defocus} occurs in the focal axis. Consequently, the FES can be generated by calculating the output signal from the detector.

$$\text{FES} = \text{PD}_A + \text{PD}_B + \text{PD}_C + \text{PD}_D. \tag{7}$$

As shown in Fig 9(e), the TES can also be generated by calculating the output signal from the detector when the relative position shift Δ_{tan} occurs in the tangential axis:

$$\text{TES} = (\text{PD}_A + \text{PD}_D) - (\text{PD}_B + \text{PD}_C). \tag{8}$$

Similarly, the RES can also be generated by calculating the output signal from the detector when the relative position shift Δ_{rad} occurs in the radial axis:

$$\text{RES} = (\text{PD}_A + \text{PD}_B) - (\text{PD}_C + \text{PD}_D). \tag{9}$$

The position of the NyA can be controlled along the focal, tangential, and radial axes by the triaxial actuator. The amount of deviation of the disc position from the expected one is acquired

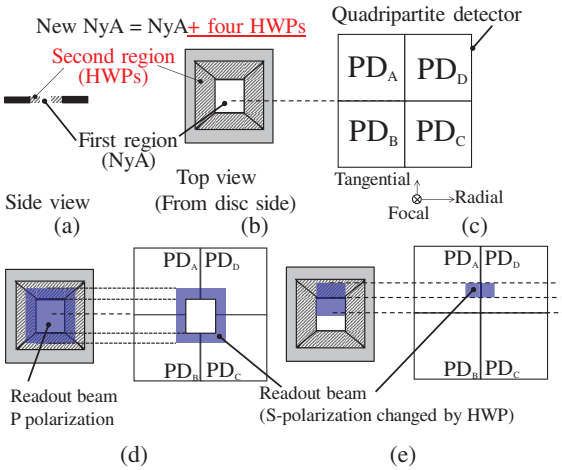

Fig. 9 Schematic illustration of situation in which the four-channel PD is illuminated as the readout beam is changed from *P* to *S* by HWP: (a) side view of NyA, (b) top view of NyA, (c) quadripartite detector with four-channel detector part and each detector name, (d) diagram of the situation in which the *S*-polarized readout beam illuminates the four-channel PD when the relative position shift Δ_{defocus} occurs in the focal axis, and (e) diagram of the situation in which the *S*-polarized readout beam illuminates the four-channel PD when the relative position shift Δ_{tan} occurs in the tangential axis.

from the intensity of a readout beam blocked by the NyA. In terabyte-class HDSSs, books are densely located in the in-plane direction of a holographic disc. There is a strong possibility that adjacent books induce crosstalk noise and decrease the accuracy of the positioning error signal when generating the positioning error signal, because reference beam angles are conventionally set to the same angular configuration in each book when recording holograms. To prevent the crosstalk noise from mixing with the positioning error signal, we make the allocation of reference beam angles different among books located next to each other when recording holograms.[32] By changing the reference beam angle, induction of crosstalk noise from an adjacent book can be suppressed.

The servo control system consists of a PD circuit, analog front end, arithmetic unit, and servo controller. The PD circuit converts each current into voltage and then amplifies the voltage signal. The function of the analog front end is to adjust the offset of the voltage signal and to reduce noise using a low-pass filter. The four-voltage signal is input into the arithmetic unit. The arithmetic unit calculates TES, RES, and FES. The TES, RES, and FES express the residual error of the reference beam from the target hologram. TES is generated by calculating a differential signal between PD_A and PD_C. In the same way, RES is generated by calculating a differential signal between PD_B and PD_D, and FES is generated by calculating the total signal of PD_A, PD_B, PD_C, and PD_D. The servo controller consists of a proportional integral derivative controller and performs feedback phase compensation for each PES. Then the position of the NyA can be shifted in each direction depending on each phase-compensated PES. As a result, the intensity of the readout beam passing the NyA is maximized.

A schematic illustration of the developed NyA unit is shown in Fig. 10. The NyA unit consists of two NyAs. One is for the recording process and does not require a moving mechanism because there is no readout beam needed to control the position of the NyA. The other NyA is for the reproduction process. It is mounted on a triaxial actuator that can be used to shift the NyA position. The actuator consists of a biaxial (focal and tangential) electromagnetic actuator and a single-axis (radial) actuator based on a stepping motor. The focus coil for moving the focal-axis actuator and the tangential coil for moving the tangential-axis actuator wind wires around a holder. The single-axis actuator consists of a stepping motor and a lead screw, and it switches the NyAs depending on the recording and reproduction process. Furthermore, during the reproduction process, the actuator adjusts the radial position based on the RES. The parameters related to the disc-positioning mechanism are summarized in Table 7.

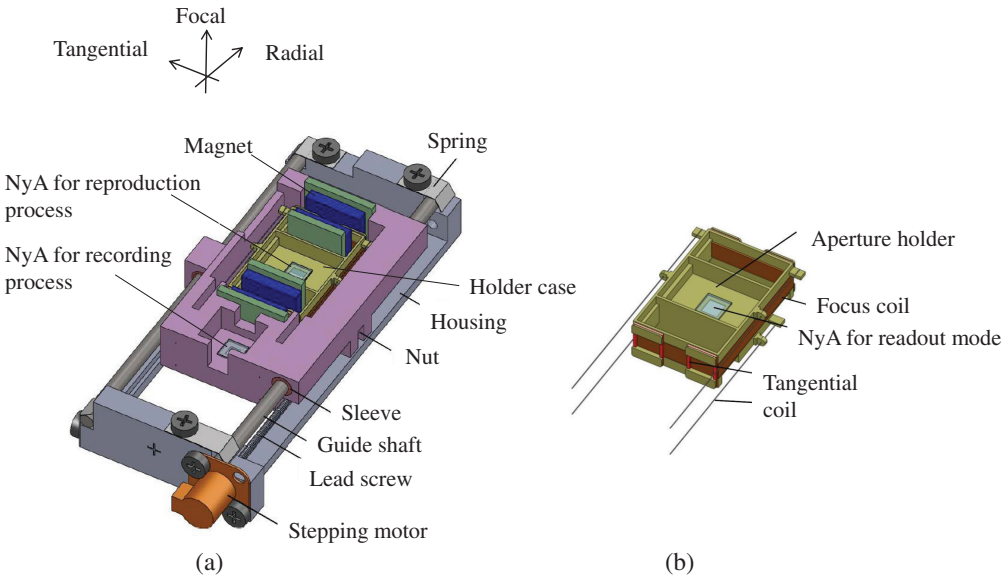

Fig. 10 Schematic illustration of NyA unit: (a) NyA unit equipped with triaxial actuator and (b) biaxial actuator holder.

Table 7 Specification of disc-positioning mechanism.

Item		Value	Unit
Sensitivity of quadripartite detector		4.5	V/μW
Moving sensitivity in focal direction		54	μm/mA
Moving sensitivity in tangential direction		14.5	μm/mA
Moving sensitivity in radial direction		0.7 in case of 1000 pps	mN · m
Spindle motor	Rotary encoder	0.012	mdeg
	Resistance	1.9	Ω
	Torque constant	13.4	mN · m/A
	Total inertia of load	0.2×10^{-3}	Kg · m^2
	Start torque	80	mN · m

4.3 *Focus Servo Control System*

Figure 11 shows each relationship between the amount of relative position shift Δ and PES obtained by the optical block. Here, $\Delta_{defocus}$, Δ_{tan}, and Δ_{rad} of the horizontal axis stand for the amount of each relative position shift of the focal, tangential, and radial axes. The vertical axis is the intensity of each PES detected by the four-channel PD. The TES and RES show a linear function for Δ_{tan} and Δ_{rad} because TES and RES indicate the bias error of the pair intensity of the readout beam detected by the four-channel PD. In contrast, the FES shows a nonlinear parabolic function for $\Delta_{defocus}$ because FES indicates the total intensity of the readout beam.

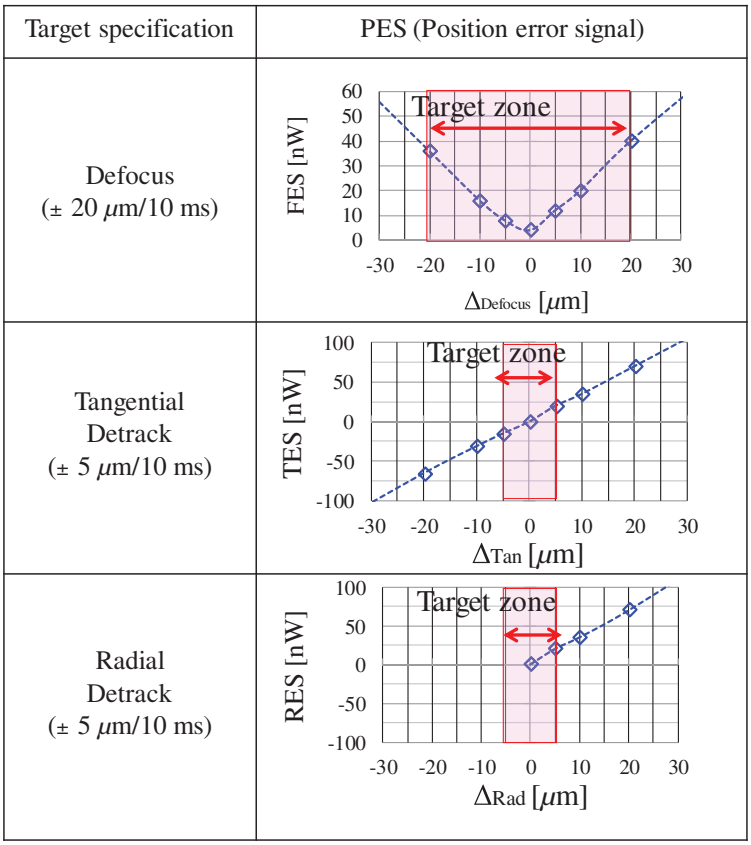

Fig. 11 Relationship between the amount of relative position shift Δ and PES.

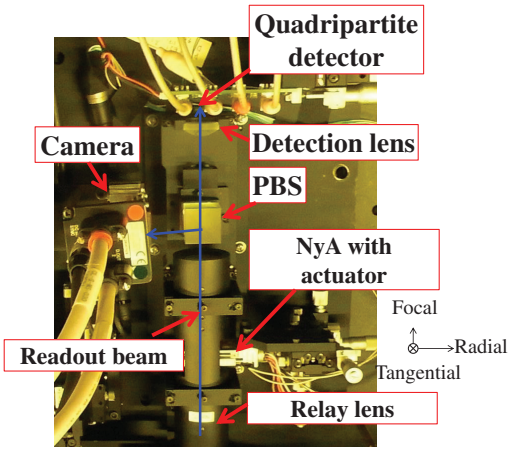

Fig. 12 Photograph of part of the experimental setup in order to verify the validity of the method of generating PESs.

In order to verify the principle of the PESs to move the NyA as shown in Fig. 11, using the experimental setup shown in Fig. 12, an experiment was performed while shifting the position of the disc independently in the three directions to change the illumination pattern of the four-channel PD. Figure 13 shows a graph of the FES generated on the basis of Eq. (7) while shifting the position of the disc in the focal direction. The white circles represent the results of calculations using data obtained from the output signals of the PD circuit of feedback control block in Fig. 7, and the black dots represent the output signals of the arithmetic unit of feedback control block in Fig. 7. The two calculated results are in good agreement. The graph showed a slight fluctuation, but the linearity required for servo control was obtained in the range of -50 to $+50$ μm, and it was confirmed that the average sensitivity was 2.0 mV/μm. Similarly, in the tangential direction, Fig. 14 shows a graph of the TES generated on the basis of Eq. (8) while shifting the position of the disc. The sensitivity calculated by linear approximation was 2.5 mV/μm. A similar experiment was performed for the last radial direction and the sensitivity was 2.0 mV/μm in Fig. 15.

To achieve a stable servo control system of the focal, tangential, and radial axes, the PES needs to have a positive or negative slope such as that of the TES or RES. In the case of the nonlinear parabolic FES, the NyA position cannot be uniquely determined from the intensity of the FES. This is because the FES gives the same value for two different NyA positions other than the origin (Δ_{defocus} is 0 μm). A conceptual diagram of the operation of a focus control using a nonlinear parabolic FES is shown in Fig. 16(a), while the relationship between FES and Δ_{defocus} is shown in Fig. 11. As shown in Fig. 4, the target specification is <20 μm and the optimum position is zero. Therefore, we intentionally shifted the operating position of the NyA from the

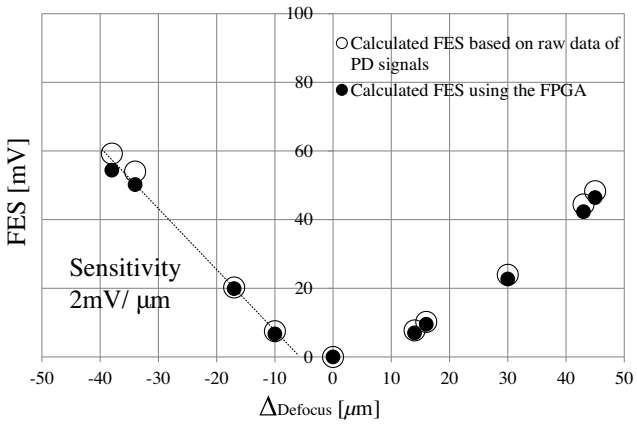

Fig. 13 FES as function of relative position shift of holographic disc in focal axis.

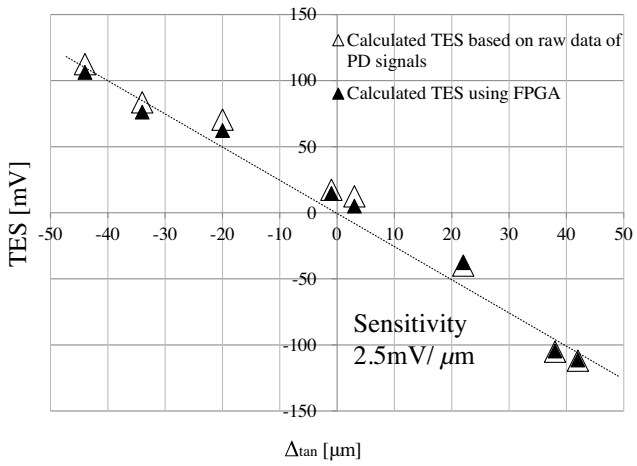

Fig. 14 TES as function of relative position shift of holographic disc in tangential axis.

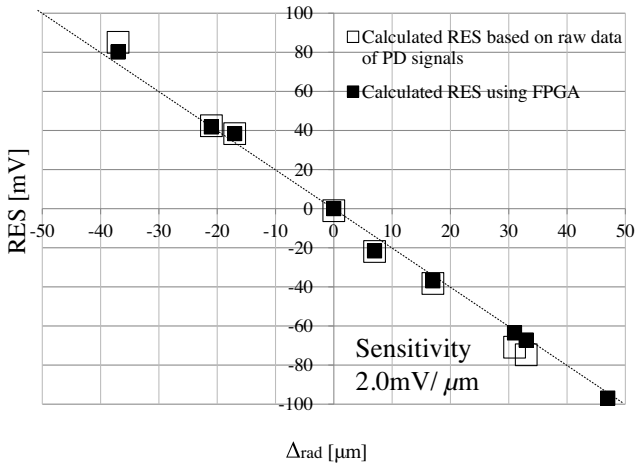

Fig. 15 RES as function of relative position shift of holographic disc in radial axis.

expected position. In the focus control system, focus pull-in control is started at the point where the FES crosses the operating position in either (I) or (II) in Fig. 16(b), and the focus control operation based on the readout beam is performed. In this case, if the intensity of the FES increases from the operating position, the focus control system controls the position of the NyA so that the intensity of the FES decreases. As a result, even though the FES is a nonlinear parabolic function, the direction to move the NyA can be uniquely determined without performing complicated linearization processing.

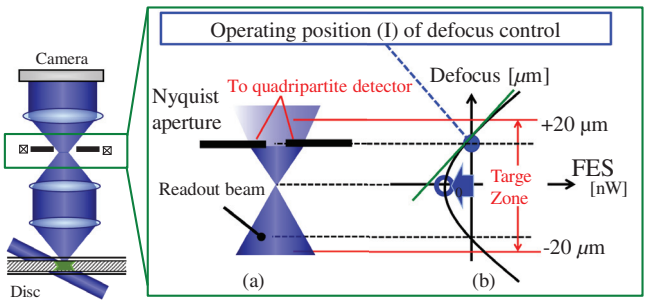

Fig. 16 Conceptual diagram of defocus control system operation: (a) relationship between NA and readout beam and (b) relationship between FES and $\Delta_{defocus}$.

5 Results and Discussion

It is necessary to identify the frequency characteristics of the triaxial actuator used to shift the NyA in order to design the settling time of the servo control system. $P_f\ (s)$ was modeled using the mass-spring-damper system, where P_f indicates the model of the plant of the focal-axis actuator. The secondary resonant frequency of the focal-axis actuator is 10.8 kHz, which does not affect the control because it is sufficiently higher than the control bandwidth (300 Hz). Therefore, $P_f\ (s)$ was modeled in consideration of the main resonance:

$$P_f(s) = \frac{\omega_n^2}{s^2 + 2\varsigma\omega_n s + \omega_n^2}, \tag{10}$$

where the main resonant frequency ω_n is 21.6 Hz and a damping factor ζ is 0.1. The frequency characteristics are shown in Fig. 17, where the solid lines indicate the model characteristics and the dotted lines indicate the results of actual measurement. The simulated and measured results are in good agreement.

A control band satisfying the target settling time of 10 ms or less with a positioning accuracy of $\pm 20\ \mu$m was estimated from the simulator of the focus control system in Fig. 18, where controller(s) is the transfer function of the controller, y_{FE} is the position of the readout beam, focusing driving signal (FOD) is the control signal for driving the focal-axis actuator the offset shifts the operating position of the NyA, D_f is the focal detection sensitivity, and the unit is V/μm. The model of the actuator given by Eq. (10) was used for $P_f(s)$ and the controller(s) was designed with a gain margin of -12 dB or more and a phase margin of 45 deg. The settling time is calculated while changing the control band of the focus control system for the unit step input corresponding to a 100-μm movement. As shown in Fig. 19, it was confirmed that a bandwidth of about 300 Hz is sufficient to satisfy the settling time of 10 ms. The control bandwidth is the frequency when the amplitude of the transfer function from input (A) to output (B) is 0 dB. The frequency was confirmed by simulation while changing the control band from 10 Hz to 2 kHz in Fig. 17.

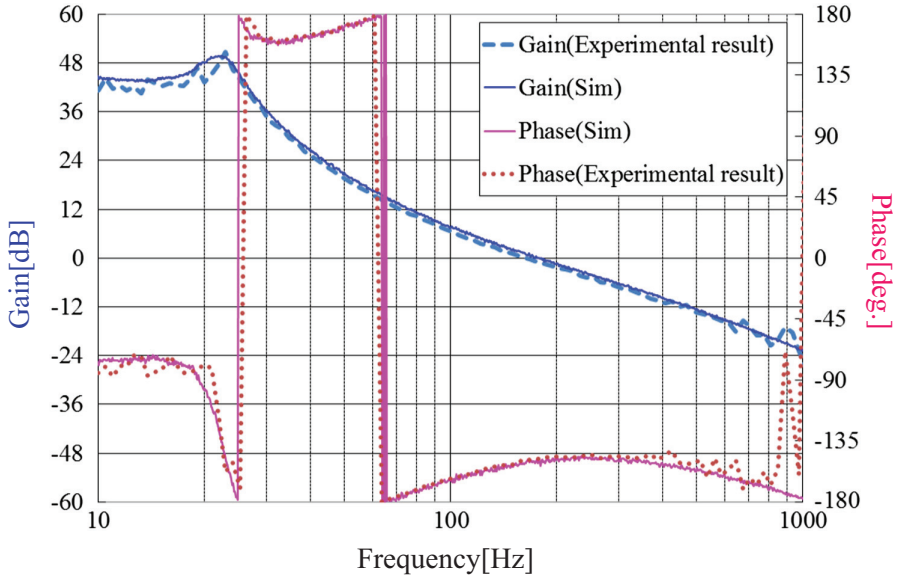

Fig. 17 Measured and simulated transfer functions of feedback control block.

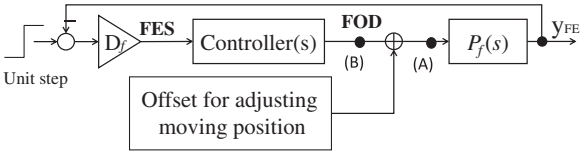

Fig. 18 Schematic diagram of focus control system.

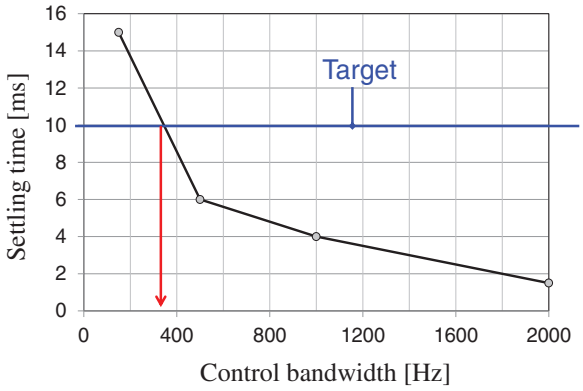

Fig. 19 Relationship between control bandwidth and settling time.

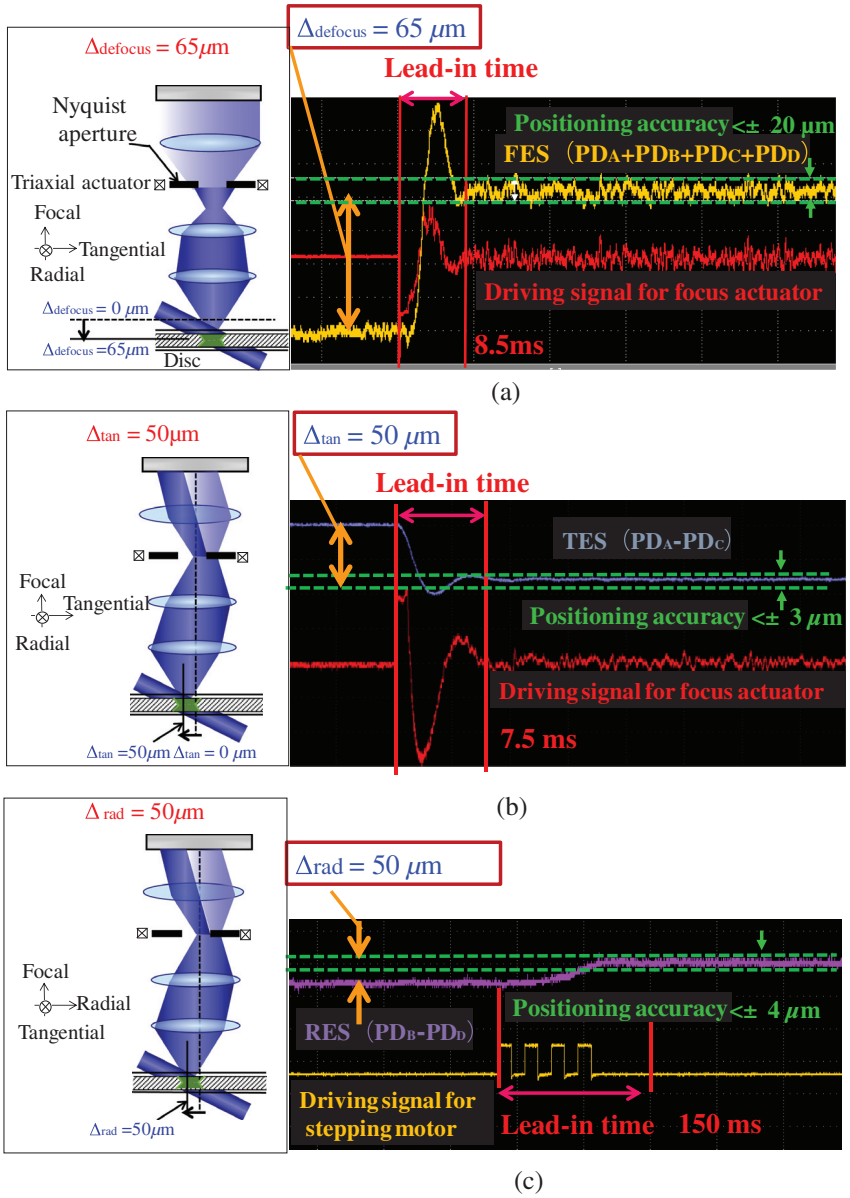

Fig. 20 Experimental result: (a) focus control system when $\Delta = 65$ μm, (b) tangential control system when $\Delta = 50$ μm, and (c) radial control system when $\Delta = 50$ μm.

Table 8 Positioning accuracy and settling time of the developed servo control system.

Control axis	Tolerance (target specification)	Settling time (target specification)
Defocus	$\pm 15\ \mu$m ($\pm 20\ \mu$m)	$\leqq$8.5 ms (10 ms)
Tangential detrack	$\pm 3\ \mu$m ($\pm 5\ \mu$m)	$\leqq$7.5 ms (10 ms)
Radial detrack	$\pm 4\ \mu$m ($\pm 5\ \mu$m)	$\leqq$150 ms (200 ms)

The result in Fig. 20(a) shows that the focus control system with the nonlinear FES was able to compensate for the relative position shift Δ_{defocus} in an experiment, where the Δ_{defocus} was 65 μm. However, the Δ_{defocus}, which occurs in the worst case due to mechanical issues, is 50 μm in our system. It shows that the focal-axis actuator was controlled with the nonlinear parabolic FES. As a result, positioning accuracy of $\pm 15\ \mu$m (= control performance of $\pm 6.8\ \mu$m and position movement of 8.5 μm) and a settling time of 8.5 ms were observed, which satisfy the requirements for the focus control system. On the other hand, the results in Figs. 20(b) and 20(c) show that the tangential and radial control system with the linear TES and RES were able to compensate for the relative position shift Δ_{tan} and Δ_{rad} in an experiment where the Δ_{tan} and Δ_{rad} were 50 μm. When Δ_{tan} and Δ_{rad} are 0 μm, the NyA is in the optimum position. Regarding tangential and radial servo control, we controlled at the optimum point. This is because the TES and RES give the unique value for the NyA position. Consequently, we confirmed that the positioning accuracy and settling time of the developed servo control system using the NyA satisfied the specifications in the HDSS, as indicated in Table 8.

6 Conclusion

We have developed a new servo control system by shifting the position of the NyA mounted on the triaxial actuator in order to control the disc position. The effectiveness of the servo system was proven from the results of optical simulation. The servo system controls the triaxial actuator by generating a real-time PES from a readout beam. The TES and RES show a linear function for Δ_{tan} and Δ_{rad}, but the FES shows a nonlinear parabolic function. With the nonlinear parabolic FES, the position of the NyA cannot be determined uniquely from the FES. The use of the focus control solves this problem without complicated linearization processing. The compensation performance was evaluated when the Δ_{defocus} was 65 μm, which occurs in the worst case due to mechanical issues. A positioning accuracy of $\pm 15\ \mu$m and settling time of 8.5 ms, which satisfy the requirements for focus, were observed. By combining new servo control system with a spindle motor, it is possible to further speed up the control. Therefore, it is highly expected that a transfer rate in the gigabit-per-second class will be achieved (Table 8).

References

1. V. Turner, "The digital universe of opportunities: rich data and the increasing value of the Internet of Things," *IDC*, 2014, https://www.emc.com/leadership/digital-universe/2014iview/executive-summary.htm (accessed 29 October 2019).
2. A. Mitsumori et al., "Multilayer 500 Gbyte optical disk," *Jpn. J. Appl. Phys.* **48**, 03A055 (2009).
3. N. Shida et al., "Multilayer optical read-only-memory disk applicable to Blu-ray disc standard using a photopolymer sheet with a recording capacity of 100 GB," *Jpn. J. Appl. Phys.* **43**, 4983–4986 (2004).
4. T. Shiono, T. Mihara, and Y. Kobayash, "Design and fabrication of thin-film diarylethene recording layer and its reflective reproduction for super-multilayered optical memories," *Jpn. J. Appl. Phys.* **46**, 3873–3877 (2007).
5. T. Kikukawa et al., "Recording characteristics of 10-layer recordable optical disc and a prospect for over 500 Gbyte recording," *Jpn. J. Appl. Phys.* **49**, 08KF01 (2010).
6. Y. Urakawa et al., "Robust adjacent track servo system with linear positioning method," *Jpn. J. Appl. Phys.* **51**, 08JA02 (2012).

7. H. Nakahara et al., "One-beam push-pull method with simple holographic optical element for multilayer Blu-ray discs," *Jpn. J. Appl. Phys.* **50**, 09MA01 (2011).
8. Y. Tanaka, T. Ogata, and S. Imagawa, "Decoupled direct tracking control system based on use of a virtual track for multilayer disk with a separate guide layer," *Jpn. J. Appl. Phys.* **54**, 09MB03 (2015).
9. Blu-Ray Disc Association 2012, "Blu-ray disc format - general 4th edition 2015," *BDA*, p. 28, 2012, http://www.blu-raydisc.com/Assets/Downloadablefile/White_Paper_General_3rd_Dec%202012_20121210.pdf (accessed 29 October 2019).
10. P. J. Van Heerden, "Theory of optical information storage in solids," *Appl. Opt.* **2**(4), 393–400 (1963).
11. D. Psaltis and G. W. Burr, "Holographic data storage," *Computer* **31**(2), 52–60 (1998).
12. H. Coufal, D. Psaltis, and G. T. Sincerbox, *Holographic Data Storage*, Part I, Springer, New York (2000).
13. K. Curtis et al., *Holographic Data Storage*, pp. 17–43, Wiley, New York (2010).
14. L. d'Auria et al., "Experimental holographic read-write memory using 3-D storage," *Appl. Opt.* **13**(4), 808–818 (1974).
15. O. Matoba and B. Javidi, "Encrypted optical storage with angular multiplexing," *Appl. Opt.* **38**(35), 7288–7293 (1999).
16. K. Anderson et al., "High speed holographic data storage at 100 Gbit/in^2," *SMPTE Motion Imaging J.* **115**(5–6), 200–203 (2006).
17. N. Kinoshita et al., "Control of angular intervals for angle-multiplexed holographic memory," *Jpn. J. Appl. Phys.* **48**, 03A029 (2009).
18. T. Muroi et al., "Compensation of interference fringe distortion due to temperature variation in holographic data storage," *Jpn. J. Appl. Phys.* **49**, 08KD03 (2010).
19. D. Psaltis et al., "Holographic storage using shift multiplexing," *Opt. Lett.* **20**(7), 782–784 (1995).
20. T. Shimura et al., "Analysis of a collinear holographic storage system: introduction of pixel spread function," *Opt. Lett.* **31**, 1208–1210 (2006).
21. L. Cao et al., "Orthogonal reference pattern multiplexing for collinear holographic data storage," *Appl. Opt.* **53**(1), 1–8 (2014).
22. K. Anderson and K. Curtis, "Polytopic multiplexing," *Opt. Lett.* **29**(12), 1402–1404 (2004).
23. I. Redmond, "The inphase professional archive drive OMA: design and function," in *Opt. Data Storage Top. Meeting*, pp. 3–5 (2006).
24. K. Tanaka et al., "415 Gbit/in.^{2} recording in coaxial holographic storage using low-density parity-check codes," in *Opt. Data Storage Top. Meeting*, pp. 64–66 (2009).
25. A. Fukumoto, "High density recording of 270 Gbit/in.^{2} in a coaxial holographic recording system," *Jpn. J. Appl. Phys.* **47**, 5891–5894 (2008).
26. T. Hoshizawa et al., "Practical angular-multiplexing holographic data storage system with 2 terabyte capacity and 1 gigabit transfer rate," *Jpn. J. Appl. Phys.* **55**, 09SA06 (2016).
27. K. Yamada et al., "High-speed reference-beam-angle control technique for holographic memory drive," *Jpn. J. Appl. Phys.* **55**, 09SA04 (2016).
28. K. Hirooka et al., "Development of a coaxial type holographic disc data storage evaluation system, capable of 500-fps-consecutive writing and reading," in *Opt. Data Storage Top. Meeting*, vol. MA4, pp. 12–14 (2006).
29. T. Ishii et al., "Margin allocation for a 500 GB holographic memory system using monocular architecture," in *Opt. Data Storage Top. Meeting*, pp. 107–109 (2009).
30. T. Ide, "Analysis of tolerances in polytopic-multiplexing holographic data storage," *Appl. Opt.* **55**, 2863–2872 (2016)
31. K. Shimada et al., "Technique for positioning hologram for balancing large data capacity with fast readout," *Jpn. J. Appl. Phys.* **56**, 09NA04 (2017).
32. Hitachi, Ltd., T. Ide and K. Shimada, "Hologram recording and recovering device and holographic recording and recovering method," US Patent US12/102966 (2009).

Yukinobu Tanaka received his PhD in engineering from Tokyo Institute of Technology. He is a researcher at the Center for Exploratory Research, R & D Group, Hitachi, Ltd., Japan. Since 2006, he has been a member of the research group working on servo control system for current

and next generation optical disc drives. His research interests include actuator control and new measurement methods using optical systems.

Tatsuro Ide joined Central Research Laboratory of Hitachi Ltd. as an optical engineer in 2002 to perform research and development of optical memory system, especially the design of optical pickup system. He worked in the development of high density recording technology enthusiastically including multilayer recording, multilevel recording and holographic recording. He is a member of the Optical Society of Japan (OSJ) and a steering committee of the Optics Design Group of OSJ.

Jiro Hashizume received his PhD in Engineering from Tokyo Institute of Technology. He is a researcher at the Center for Technology Innovation, R & D Group, Hitachi, Ltd., Japan. Since 2006, he has been a member of the research group working on mechanical systems for current and next generation optical disc drives. His research interests include actuators and sensors for optical systems and robotics.